SUPPORTING INFORMATION

Identification and Characterization of ML321: a Novel and Highly Selective D_2 Dopamine Receptor Antagonist with Efficacy in Animal Models that Predict Atypical Antipsychotic Activity

R. Benjamin Free[a], Ashley N. Nilson[a], Noelia M. Boldizsar[a], Trevor B. Doyle[a,&], Ramona M. Rodriguiz[b], Vladimir M. Pogorelov[b], Mayako Machino[c,#], Kuo Hao Lee[c], Jeremiah W. Bertz[d+], Jinbin Xu[e], Herman D. Lim[f,^], Andrés E. Dulcey[g], Robert H. Mach[h], James H. Woods[d,$], J. Robert Lane[i], Lei Shi[c], Juan J. Marugan[g], William C. Wetsel[b,j], David R. Sibley[a*]

[a]Molecular Neuropharmacology Section, National Institute of Neurological Disorders and Stroke, Intramural Research Program, National Institutes of Health, 35 Convent Drive, MSC-3723, Bethesda, MD, 20892, United States. [b]Department of Psychiatry and Behavioral Sciences, Mouse Behavioral and Neuroendocrine Analysis Core Facility, Duke University Medical Center, 354 Sands Building, 303 Research Drive, Durham, NC, 27710, United States. [c]Computational Chemistry and Molecular Biophysics Section, Molecular Targets and Medications Discovery Branch, National Institute on Drug Abuse, Intramural Research Program, National Institutes of Health, 333 Cassell Drive, Baltimore, MD 21224, United States. [d]Department of Pharmacology, University of Michigan Medical School, 1150 W. Medical Center Dr., Ann Arbor, MI 48109, United States. [e]Division of Radiological Sciences, Department of Radiology, Mallinckrodt

Institute of Radiology, Washington University School of Medicine, St. Louis, MO, USA. [f]Drug Discovery Biology, Monash Institute of Pharmaceutical Sciences, Monash University, 399 Royal Parade, Parkville, VIC 3052, Australia. [g]Division of Pre-Clinical Innovation, National Center for Advancing Translational Sciences, National Institutes of Health, 9800 Medical Center Drive, Rockville, MD 20850, United States. [h]Department of Radiology, Perelman School of Medicine, University of Pennsylvania, 3400 Civic Center Boulevard, Philadelphia, PA 19104, United States. [i]Centre of Membrane Proteins and Receptors, Universities of Birmingham and Nottingham, Nottingham, NG7 2UH, United Kingdom. [j]Departments of Neurobiology and Cell Biology, Duke University Medical Center, 354 Sands Building, 303 Research Drive, Durham, NC, 27710, United States.

*Corresponding author: David R. Sibley, Molecular Neuropharmacology Section, National Institute of Neurological Disorders and Stroke, Intramural Research Program, National Institutes of Health, 35 Convent Drive, MSC-3723, Bethesda, MD, 20892, United States. Email: sibleyd@ninds.nih.gov.

TABLE OF CONTENTS

Supporting Figures

Figure S1. Functional profiling of ML321 against an array of 168 known GPCRs. The data are from **Figures 2A** and **B**, representing the panel screens with ML321 in antagonist and agonist modes, respectively. GPCRs of interest include $D2R_S$ (DRD2S), $D2R_L$ (DRD2L), D3R (DRD3), 5-HT_{2A} serotonin (HTR2A), 5-HT_{2C} serotonin (HTR2C), BLT1 (leukotriene B_4) (LTB4R), sphingosine-1-phosphate 4 (S1PR4), α_{2C}-adrenergic (ADRA2C), and CB2 cannabinoid (CB2).

Antagonist mode:

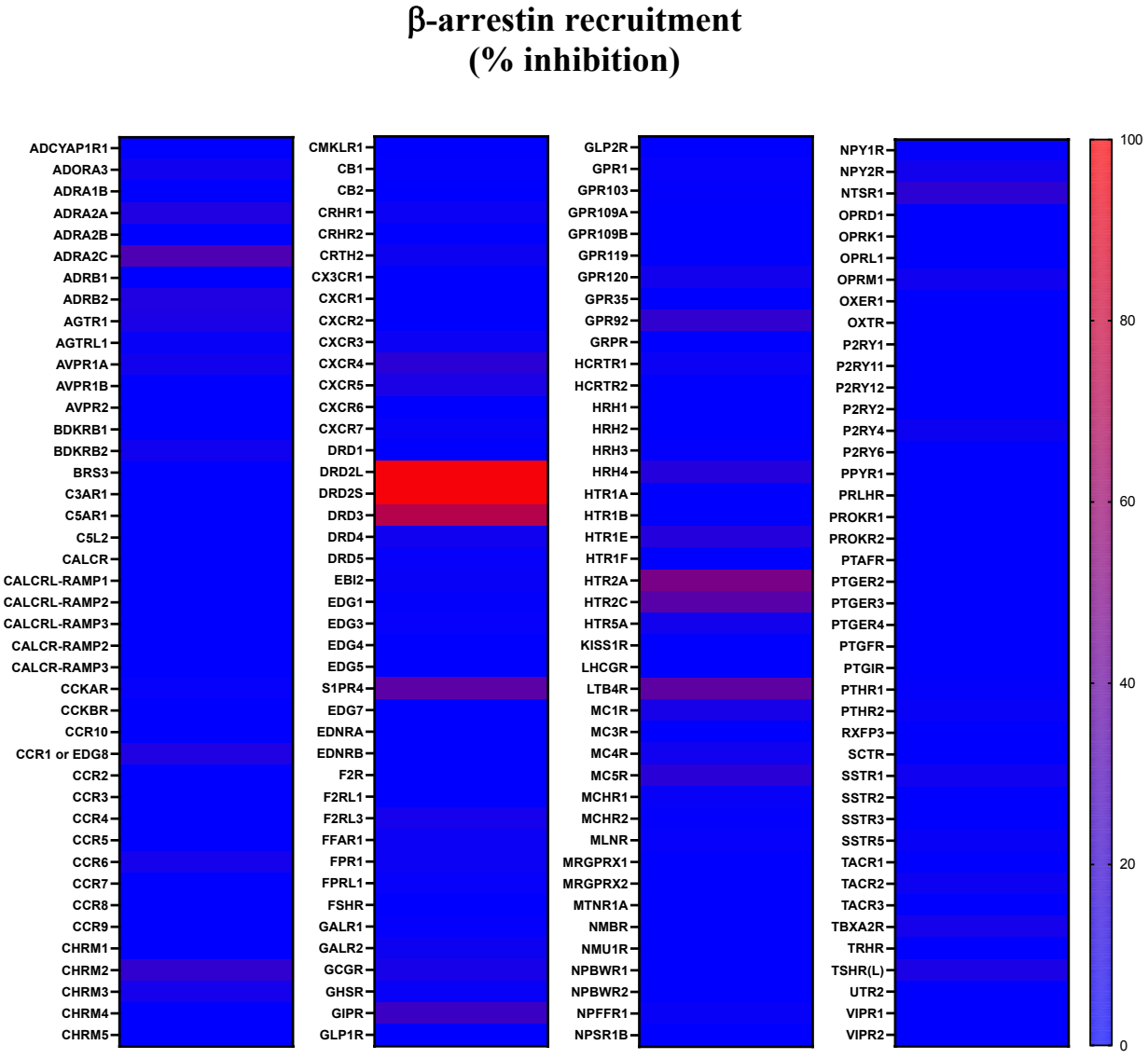

Agonist mode:

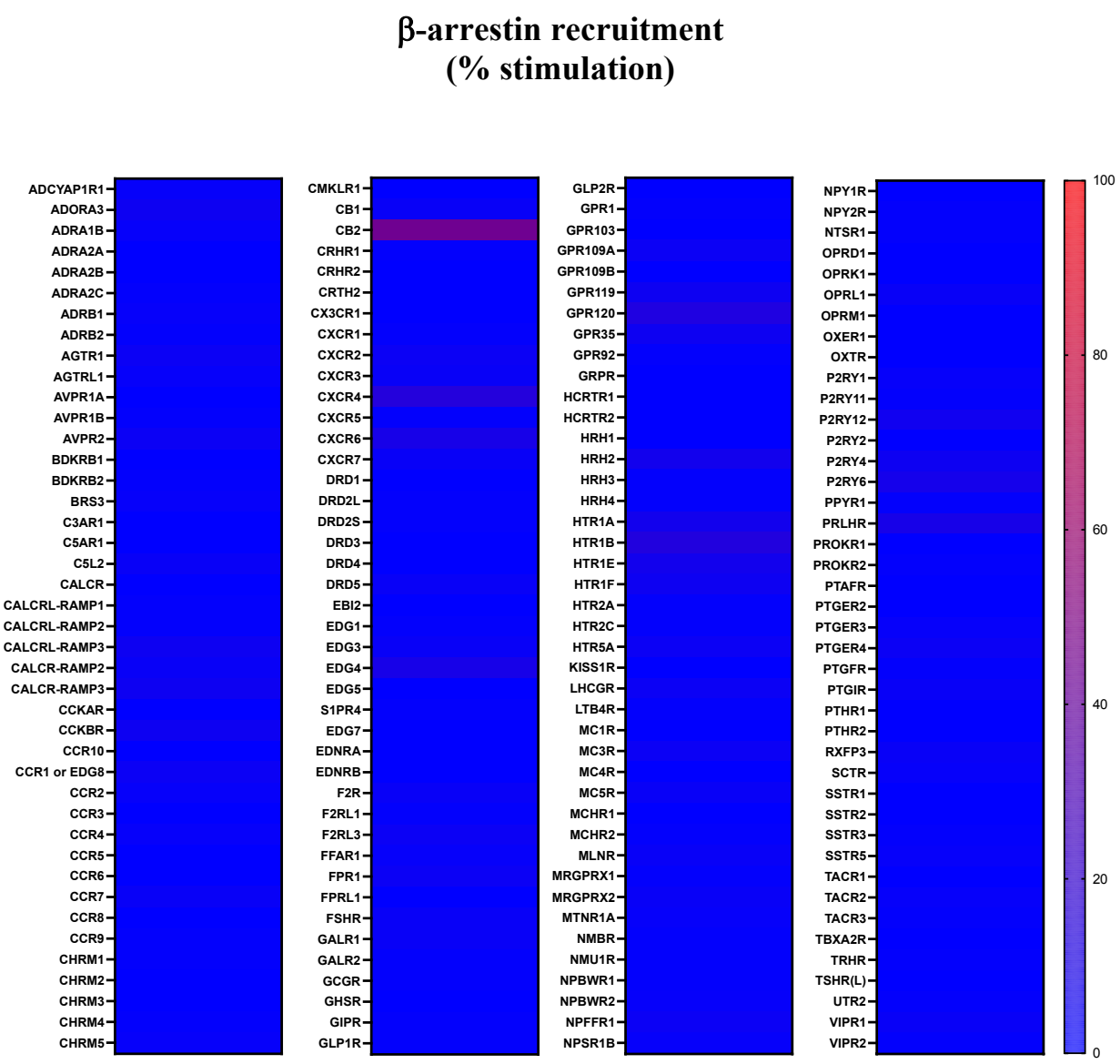

Figure S2. ML321 is a competitive antagonist of D2R-mediated β-arrestin recruitment and Go protein activation. Curve-shift assays were conducted by stimulating the receptor with the indicated concentrations of dopamine with or without various concentrations of ML321. Data are expressed as Δ BRET from baseline, which represents the constitutive BRET signal seen in the absence of any drug treatment. Insets represent Schild regression analyses of the data that were used to calculate mean K_B values [95% C.I.]. (**A**) Dopamine-stimulated β-arrestin recruitment was assessed using a BRET-based assay as described in *Methods*. A representative experiment performed in triplicate is shown. ML321 K_B = 239 nM [81-397] (N = 3). (**B**) D2R-mediated Go activation was measured using a BRET-based assay as described in *Methods*. A representative experiment performed in triplicate is shown. ML321 K_B = 143 nM [10.1-441] (N = 3).

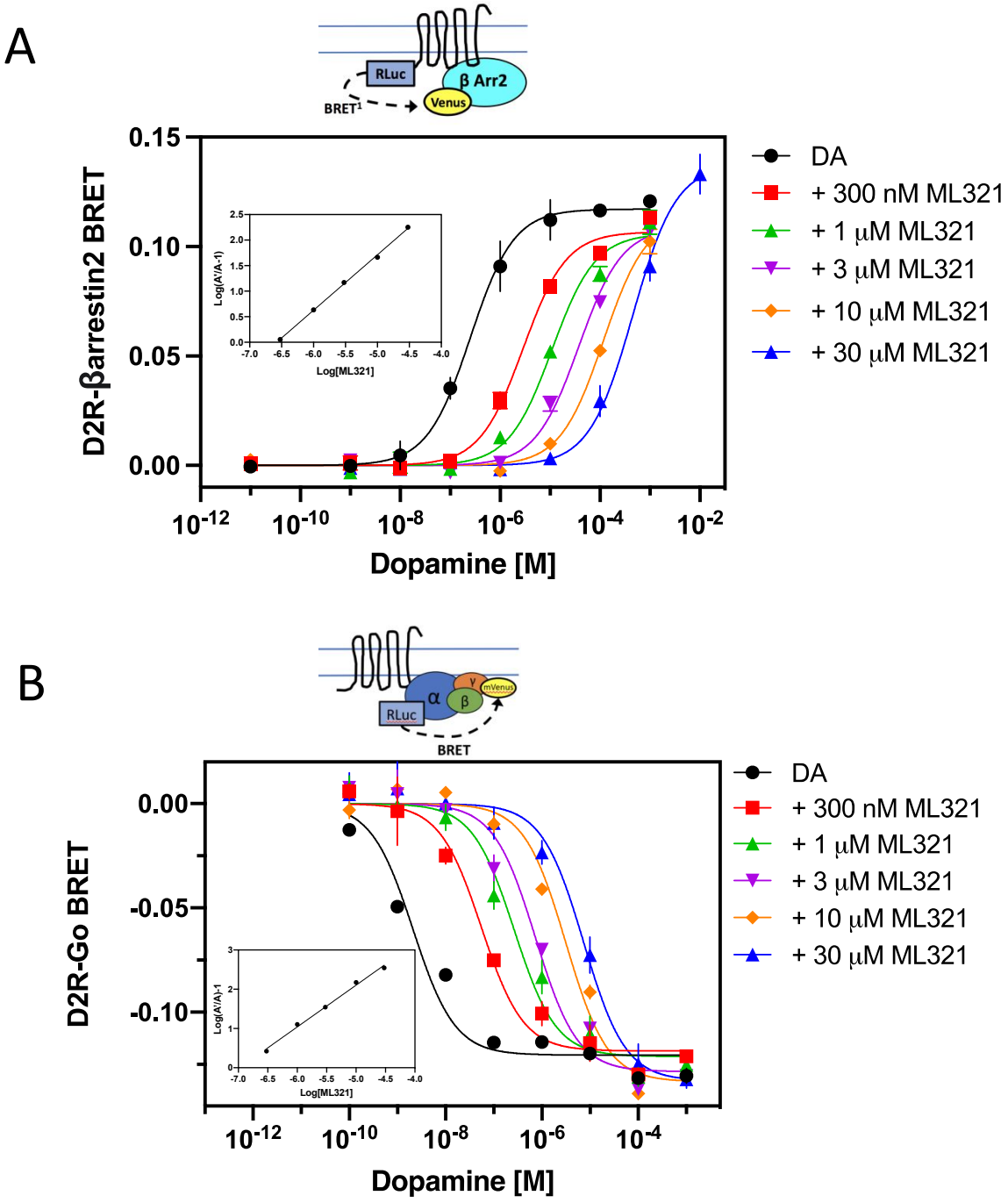

Figure S3. ML321 exhibits inverse agonist activity at the D2R in a concentration-dependent manner. Go BRET assays were performed as described in **Figure 4** (see legend). Data represent the mean ± SEM of five independent experiments performed in triplicate that are expressed as Δ BRET from baseline (zero), which represents the BRET signal seen in the absence of drug treatment. The mean ML321 EC_{50} value [95% C.I.] = 275 nM [32 nM - 6 μM] (N = 5).

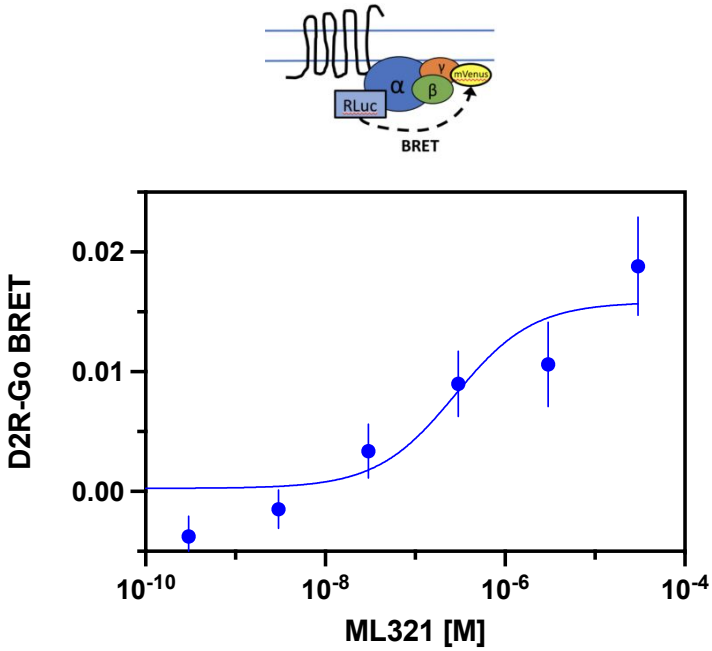

Figure S4. Null and startle activities in the prepulse inhibition experiment shown in **Figure 10**. The study was performed as described in the legend for **Figure 10** and in the *Methods*. (**A**) For null activity with amphetamine, a one-way ANOVA found treatment to be significant [$F(6,61)=8.165$, $p<0.001$]. **(B)** Similarly, for startle activity with amphetamine, the one-way ANOVA determined the treatment effect was significant [$F(6,61)=5.092$, $p<0.001$]. (**C**) In the phencyclidine experiment, a one-way ANOVA for null activity detected significant treatment effects [$F(6,61)=7.374$, $p<0.001$]. (**D**) For startle activities in the phencyclidine study, a one-way ANOVA identified the treatment effect to be significant [$F(6,61)=3.011$, $p=0.012$]. The data are presented as means ± SEMs. N=9 mice for the Veh-Veh, Veh-AMPH, and Veh-PCP groups; N=10 mice for all other groups. $^{\dagger}p<0.05$, for the AMPH startle study (startle activity) 5 mg/kg ML321(ML)-Veh *vs.* the Veh-Veh group; $*p<0.05$, Veh-AMPH or Veh-PCP *vs.* the indicted groups; $^{\#}p<0.05$, 0.25 mg/kg ML-AMPH or ML-PCP *vs.* the indicated groups; $\wedge p<0.05$, 0.5 mg/kg ML-AMPH or ML-PCP *vs.* the indicated groups; $^{+}p<0.05$, 1 mg/kg ML-AMPH or ML-PCP *vs.* the indicated groups; $^{\ddagger}p<0.05$, for the PCP study (null activity) 5 mg/kg ML-PCP *vs*. the Veh-Veh and 5 mg/kg ML-Veh groups.

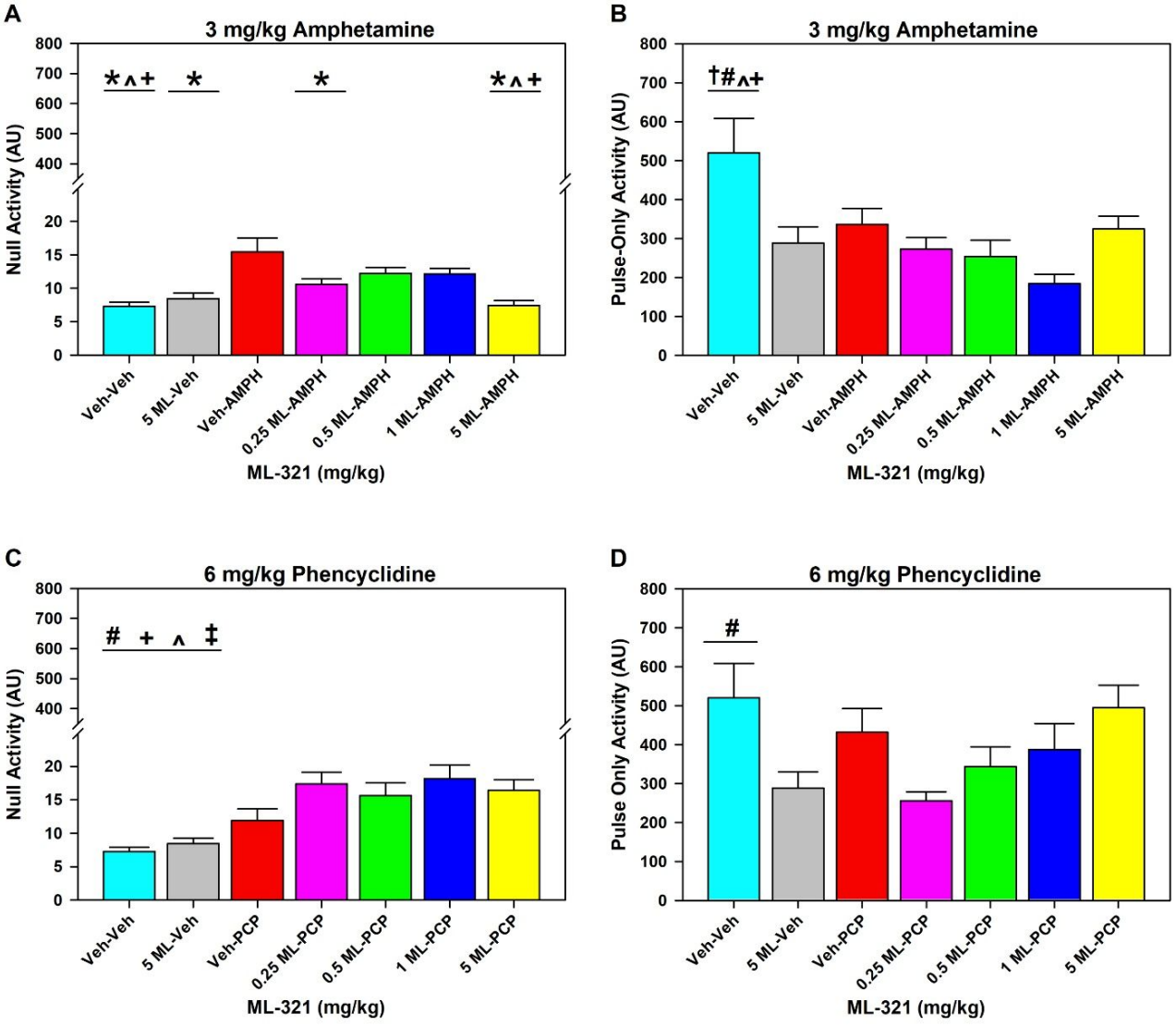

Figure S5. Catalepsy assessed using the inclined screen test. C57BL/6J mice were injected (i.p.) with vehicle or a 10 mg/kg dose of either haloperidol (HAL) or ML321 (ML). Mice were returned to their home cages and then tested 30 and 60 min later for catalepsy. In this test, the mice were initially placed face-down on a horizontal wire-mesh screen that was inclined at a 45° angle, and the latency to move the four paws (**A**) or one body length (**B**) was recorded with a 300 sec cut-off. The data are presented as means and SEMs. N=10 mice/group. A RMANOVA detected a significant treatment effect to move 4 paws [$F(1,18)=23.389$, $p<0.001$] and to move 1 body length [$F(1,18)=46.590$, $p<0.001$]. The data are presented as means ± SEMs. N=10 mice for all groups. *$p<0.05$, HAL *vs.* ML.

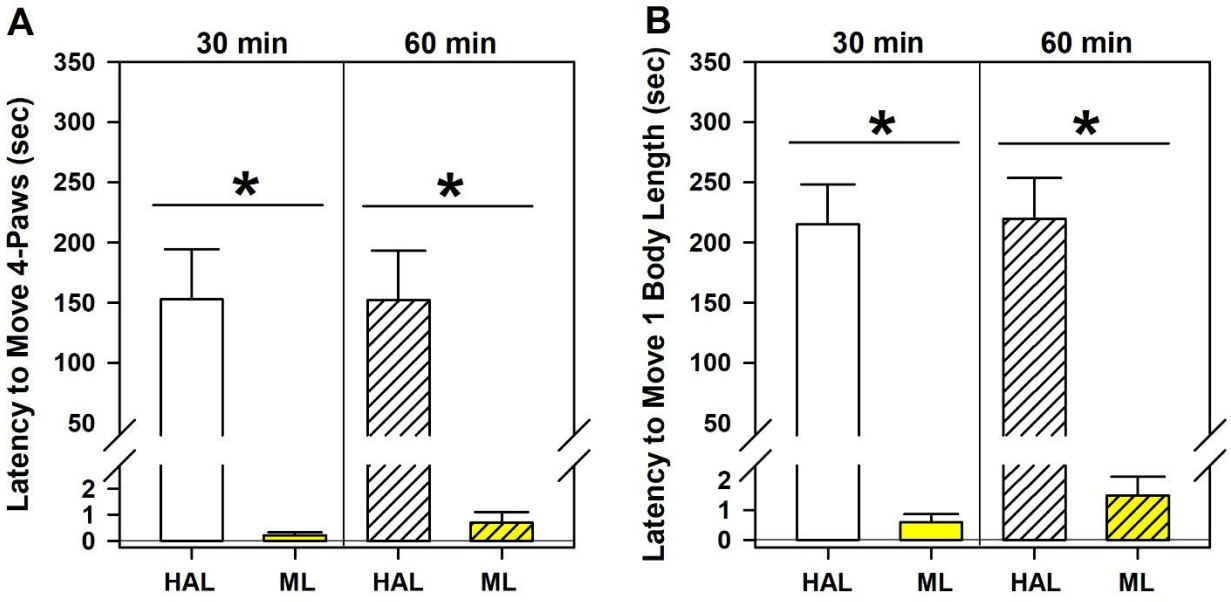

Supporting Tables

Table S1. Results from the Psychoactive Drug Screening Program (PDSP) assay[a]

Target	**ML321** (10 µM) **% Inhibition**	Target	**ML321** (10 µM) **% Inhibition**
5HT1A	NA[b]	D2	**92**
5HT1B	NA	D3	**59**
5HT1D	NA	D4	NA
5HT1E	NA	D5	NA
5HT2A	NA	DAT	NA
5HT2B	NA	DOR	NA
5HT2C	**64**	$GABA_A$	NA
5HT3	NA	H1	NA
5HT4	NA	H2	NA
5HT5A	NA	H3	NA
5HT6	NA	H4	NA
5HT7	**53**	KOR	NA
Alpha1A	NA	M1	NA
Alpha1B	NA	M2	NA
Alpha1D	NA	M3	NA
Alpha2A	NA	M4	NA
Alpha2B	NA	M5	NA
Alpha2C	NA	MOR	NA
Beta 1	NA	NET	NA
Beta 2	NA	PBR	NA
Beta 3	NA	SERT	NA
BZP site	NA	Sigma 1	NA
D1	NA	Sigma 2	NA

[a] Radioligand binding assays were performed as described in the Methods. Data are from **Figure 1C** and represent the percent inhibition by ML321 of radioligand binding to each target.
[b] NA indicates inhibition of binding was <50% in the primary assay that was performed using a single (10 μM) concentration of ML321.

Table S2. Functional profiling of ML321 using the DiscoverX gpcrMAX^{TM} assay panel as described in **Figure 2**. GPCRs of interest include $D2R_S$ (DRD2S), $D2R_L$ (DRD2L), D3R (DRD3), 5-HT_{2A} serotonin (HTR2A), 5-HT_{2C} serotonin (HTR2C), BLT1 (leukotriene B_4) (LTB4R), sphingosine-1-phosphate 4 (S1PR4), α_{2C}-adrenergic (ADRA2C), and CB2 cannabinoid (CB2).

Panel key (GPCR list):

	1	2	3	4	5	6	7	8	9	10	11	12	13	14	15	16	17	18	19	20	21
A	ADCYAP1R1	AGTR1	C3AR1	CALCR-RAMP3	CCR5	CHRM4	CX3CR1	DRD1	EDG3	F2RL1	GCGR	GPR10B	HRH1	HTR2A	MC4R	NMBR	NTSR1	P2RY11	PROKR2	PTHR2	TACR2
B	ADORA3	AGTRL1	C5AR1	CCKAR	CCR6	CHRM5	CXCR1	DRD2L	EDG4	F2RL3	GHSR	GPR119	HRH2	HTR2C	MC5R	NMU1R	OPRD1	P2RY12	PTAFR	RXFP3	TACR3
C	ADRA1B	AVPR1A	C5L2	CCKBR	CCR7	CMKLR1	CXCR2	DRD2S	EDG5	FFAR1	GIPR	GPR120	HRH3	HTR5A	MCHR1	NPBWR1	OPRK1	P2RY2	PTGER2	SCTR	TBXA2R
D	ADRA2A	AVPR1B	CALCR	CCR10	CCR8	CB1	CXCR3	DRD3	S1PR4	FPR1	GLP1R	GPR35	HRH4	KISS1R	MCHR2	NPBWR2	OPRL1	P2RY4	PTGER3	SSTR1	TRHR
E	ADRA2B	AVPR2	CALCRL-RAMP1	CCR1 or EDG8	CCR9	CB2	CXCR4	DRD4	EDG7	FPRL1	GLP2R	GPR92	HTR1A	LHCGR	MLNR	NPFFR1	OPRM1	P2RY6	PTGER4	SSTR2	TSHR(L)
F	ADRA2C	BDKRB1	CALCRL-RAMP2	CCR2	CHRM1	CRHR1	CXCR5	DRD5	EDNRA	FSHR	GPR1	GRPR	HTR1B	LTB4R	MRGPR1	NPSR1B	OXER1	PPYR1	PTGFR	SSTR3	UTR2
G	ADRB1	BDKRB2	CALCRL-RAMP3	CCR3	CHRM2	CRHR2	CXCR6	EBI2	EDNRB	GALR1	GPR103	HCRTR1	HTR1E	MC1R	MRGPR2	NPY1R	OXTR	PRLHR	PTGIR	SSTR5	VIPR1
H	ADRB2	BRS3	CALCR-RAMP2	CCR4	CHRM3	CRTH2	CXCR7	EDG1	F2R	GALR2	GPR10A	HCRTR2	HTR1F	MC3R	MTNR1A	NPY2R	P2RY1	PROKR1	PTHR1	TACR1	VIPR2

Antagonist Mode results from **Figure 2A**:

	1	2	3	4	5	6	7	8	9	10	11	12	13	14	15	16	17	18	19	20	21
A	-2%	10%	-10%	-7%	0%	-3%	-2%	-5%	2%	-2%	9%	-11%	-9%	48%	6%	-14%	17%	-2%	-9%	3%	5%
B	6%	3%	-1%	2%	8%	-14%	0%	98%	-7%	8%	3%	-3%	-13%	35%	16%	-5%	-3%	-14%	-4%	-4%	-2%
C	-1%	7%	-6%	-3%	-5%	-4%	-24%	98%	-10%	4%	23%	7%	1%	7%	3%	-9%	-7%	-7%	-3%	-11%	8%
D	12%	-6%	-14%	0%	-12%	1%	4%	72%	36%	4%	-7%	-8%	14%	-3%	1%	-2%	-9%	5%	-8%	6%	-18%
E	-16%	-8%	-6%	12%	-3%	-7%	16%	6%	-4%	2%	-6%	19%	-1%	-9%	2%	3%	6%	-8%	-2%	-6%	10%
F	31%	-9%	-4%	-6%	-1%	4%	10%	2%	-2%	-25%	2%	-2%	-1%	37%	-9%	-17%	-26%	-2%	-1%	-5%	-3%
G	-7%	6%	-6%	-23%	19%	-4%	0%	3%	-11%	1%	1%	4%	14%	9%	-18%	1%	-5%	-16%	-12%	3%	-1%
H	12%	-22%	-16%	-2%	8%	5%	3%	1%	-7%	5%	-26%	-4%	0%	-17%	-1%	7%	-1%	-1%	1%	-13%	-4%

Agonist mode results from **Figure 2B**:

	1	2	3	4	5	6	7	8	9	10	11	12	13	14	15	16	17	18	19	20	21
A	2%	4%	0%	5%	0%	1%	0%	0%	3%	1%	1%	0%	0%	1%	0%	1%	1%	1%	1%	0%	2%
B	5%	2%	0%	0%	0%	2%	1%	1%	9%	4%	-4%	5%	7%	1%	3%	1%	0%	6%	0%	3%	1%
C	2%	0%	3%	5%	3%	0%	4%	1%	0%	2%	1%	12%	1%	4%	-1%	1%	-3%	0%	-2%	2%	0%
D	-2%	1%	0%	-2%	0%	3%	3%	-4%	1%	4%	1%	5%	1%	0%	1%	2%	3%	5%	2%	-1%	1%
E	-3%	4%	1%	4%	1%	44%	14%	0%	0%	0%	0%	1%	7%	4%	3%	4%	0%	8%	4%	0%	-1%
F	1%	-1%	1%	2%	1%	1%	1%	3%	0%	3%	1%	0%	13%	1%	1%	2%	0%	1%	1%	1%	1%
G	2%	1%	5%	0%	0%	0%	9%	0%	0%	3%	-11%	0%	7%	0%	3%	0%	0%	9%	3%	2%	3%
H	1%	2%	3%	2%	0%	-2%	3%	1%	3%	1%	4%	0%	5%	4%	2%	1%	2%	0%	0%	0%	1%

Table S3. Impact of D2R point mutations on ML321 antagonist potencies as assessed using dopamine-stimulated Go BRET activation assays.

Mutant D2R	Dopamine Mutant EC_{50}/WT EC_{50} ± SEM	ML321 Mutant IC_{50}/WT IC_{50} ± SEM
$V91^{2.61}A$	1.23 ± 0.39	**4.87 ± 1.2***
$L94^{2.64}A$	**3.34 ± 0.71***	**2.24 ± 0.33***
$W100^{EL1.50}A$	**15.0 ± 5.8***	**>40**[#]
$F110^{3.28}A$	**24.7 ± 6.65***	**0.20 ± 0.05***
$T119^{3.37}A$	ND	ND
$I184^{EL2.52}A$	**36.8 ± 4.12***	**1.77 ± 0.24***
$S197^{5.46}A$	ND	ND
$F390^{6.52}A$	**9.1 ± 4.11***	**>40**[#]
$H393^{6.55}A$	**39.6 ± 13.9***	1.32 ± 0.26

Go-BRET activation assays were performed using the wild-type (WT) or mutant D2Rs as described in the Methods. Concentration-response curves (CRCs) were first performed for dopamine to determine the EC_{50} and EC_{80} values for each mutant receptor. Subsequently, cells expressing each mutant receptor were stimulated with an EC_{80} concentration of dopamine and ML321 CRCs were performed to determine the IC_{50} values for antagonism of this response. In each experiment, the dopamine EC_{50} or ML321 IC_{50} values for the mutant D2Rs were divided by their values for the WT D2R to assess the fold-change, if any, resulting from the mutation. The data shown represent the mean ± SEM values from 3-4 experiments each performed in triplicate. ND indicates that the mutation was severely deleterious to dopamine activity and thus not determinable. [#]Indicates that the ML321 CRC was incomplete at the highest concentration tested (10 μM) ***$p < 0.05$** indicates significantly different from unity (1.0) as determined statistically using the one sample t test.

Table S4. Impact of D2R point mutations on ML321 binding affinities as assessed using [^{3}H]-methylspiperone competition binding assays.

Mutant D2R	Spiperone Mutant Ki/WT Ki ± SEM	ML321 Mutant Ki/WT Ki ± SEM
V91$^{2.61}$A	ND	ND
L94$^{2.64}$A	1.61 ± 0.23	1.96 ± 1.04
W100$^{EL1.50}$A	ND	ND
F110$^{3.28}$A	0.95 ± 0.23	**0.05 ± 0.02***
T119$^{3.37}$A	2.04 ± 0.87	0.92 ± 0.31
I184$^{EL2.52}$A	0.99 ± 0.11	1.71 ± 0.34
S197$^{5.46}$A	0.86 ± 0.42	0.58 ± 0.1
F390$^{6.52}$A	1.36 ± 0.19	**19.04 ± 5.2***
H393$^{6.55}$A	1.40 ± 0.38	**9.77 ± 2.9***

Radioligand binding competition assays for spiperone and ML321 were performed using the wild-type (WT) or mutant D2Rs as described in the Methods. IC_{50} values were determined for each competing ligand and used to calculate Ki values using the Cheng-Prusoff equation[50]. In each experiment, the ligand Ki values for the mutant D2Rs were divided by their values for the WT D2R to assess the fold-change, if any, resulting from the mutation. The data shown represent the mean ± SEM values from 3-4 experiments each performed in triplicate. ND indicates that the mutation was deleterious to [^{3}H]-methylspiperone binding and thus not determinable. *$p < 0.05$ indicates significantly different from unity (1.0) as determined statistically using the one sample t test.

Supplemental Files:

ML321-D2R MD simulation.mpg

A representative molecular dynamics simulation trajectory showing the binding pose of ML321 in the D2R. The carbon atoms of ML321 are in orange, while the receptor contact residues mutated in this study are in green. The sulfur atom of ML321's thiophene ring is in yellow. Note that the sidechains of I184$^{EL2.52}$, F389$^{6.51}$, and F390$^{6.52}$ (in spheres) tightly accommodate the tricyclic dibenzothiazepine moiety of ML321 in the orthosteric binding site, while the bulky phenyl sidechain of F110$^{3.28}$ pushes back and forth with the thiophene ring in the secondary binding pocket.